Advances in Engineering Software 42 (2011) 25–34

Contents lists available at ScienceDirect

Advances in Engineering Software

journal homepage: www.elsevier.com/locate/advengsoft

# Simulated wave-driven ANN model for typhoon waves

Hsien-Kuo Chang [a], Jin-Cheng Liou [a,*], Shen-Jung Liu [b,c], Shyne-Ruey Liaw [b]

[a] Department of Civil Engineering, National Chiao Tung University, Hsinchu 300, Taiwan
[b] CECI Engineering Consultants, Inc., Taiwan
[c] Department of Civil Engineering, National Taiwan University, Taipei, Taiwan

ARTICLE INFO

*Article history:*
Received 1 March 2010
Received in revised form 16 July 2010
Accepted 4 October 2010
Available online 12 November 2010

*Keywords:*
MIKE21_SW
Artificial neural network
Typhoon waves
Vortex wind model
NCEP wind field
Hybrid wave model

ABSTRACT

This paper investigates an artificial neural network (ANN) model for typhoon waves used to modify poor calculations of the numerical model in special cases. Two key factors, local winds and simulated waves produced by the numerical model, were used as input parameters of the proposed ANN model. The waves were simulated by the numerical model from a wave action equation indicating the physical processes of energy transfer and wave propagation. Simulated wave input is a very important parameter for the proposed ANN model, allowing for the accurate calculation of water waves in the sea. The applicable Mike21_SW model was chosen to provide an accurate calculation. Through model verification, the proposed ANN model has a particularly accurate calculation at the peak of each typhoon and at its occurrence time. The computed waves of each typhoon were examined to be consistent with the observed waves.


## 1. Introduction

Information on swell and wind waves is very important for marine activities and for safe navigation. Therefore, some engineers and scientists have devoted their time to the study of the accurate calculation of water waves in the sea. Initially simple empirical prediction models, such as SMB (Sverdrup–Munk–Bretschneider) and Joint North Sea Wave Atmosphere Program (JONSWAP), were proposed to provide a quick but defective estimation of ocean waves [1,2]. The drawback attributes to that waves depend not only on the present wind field but also on earlier wind fields, bathymetric effect, pre-existing waves from other wind systems, and in general on the entire wave-generation process over the last to 12–24 h. With the help of fast computer calculations and the knowledge of physical processes responsible for wave behavior, numerical simulation studies were developed as first and second generation wave models. First-generation models that have been modified to allow the Phillips equilibrium coefficient to vary dynamically [3] and second-generation models [4] have been shown to produce good predictions and hindcasts of wave conditions for a wide range of metrological situations. However, these wave models were found to be limited to extreme situations.

At the same time, new numerical improvements in computations of Boltzmann-type integrals provided a powerful tool to overcome the numerical difficulties of the second generation wave models. These improvements were used in the third generation models developed by the WAMDI (the wave model development and implementation) group [5]. The basic version of this type of wave model was developed for deep water waves by Hasselmann et al. [6] and was termed WAM. An application, especially for nearshore wave and current conditions, was developed as the WAM deep water model. This model was described by Booij et al. [7] and Ris et al. [8] and was named the SWAN-model. The final report on these efforts was published by Komen et al. [9]. Hsu et al. [10] used finite element method (FEM) in SWAN to simulate water waves in the nearshore zone. There were two particularly important features of the third generation model. The first was the parameterization of the exact non-linear transfer source function, which contained the same number of degrees of freedom as the spectrum itself. The second was the energy balance closed by specifying the unknown dissipation source function.

To illustrate a general feature of the global wave hindcast, extensive verification of the third generation wave model WAM was reported by Romeiser [11]. WAM wave heights were compared with GEOSAT radar altimeter data for the entire year of 1988 for the southern hemisphere and the tropical region. These data were found to be underestimated by up to approximately 30% from May through September. Because of the complicated oceanography of the region, the accuracy of the wind input fields plays a critical role in the performance of the wave model. This technique is called assimilation analysis. In assessing the spectral wind wave modelling, Liu et al. [12] compared four numerical models and concluded that the models reflected similar general

* Corresponding author. Tel./fax: +886 3 5131487.
*E-mail address:* jcliou.cv87g@nctu.edu.tw (J.-C. Liou).

0965-9978/$ - see front matter © 2010 Elsevier Ltd. All rights reserved.
doi:10.1016/j.advengsoft.2010.10.014

trends and patterns, although the differences between the calculated results and observations were of the equivalent orders of magnitude. It was also pointed out that imperfect specification of the wind field is a limiting factor for producing accurate wave model results, but it is often hard to separate wind and wave model errors. Therefore, there is still a requirement for new wave forecasting techniques rather than pure wave modelling.

Taiwan is an island that is 385 km long in the north–south direction and 143 km wide in the east–west direction. Approximately two-thirds of the island is covered with lush forested mountains which are approximately 2000–4000 m above sea level. Indeed, these high mountains in Taiwan play an important role in changing the wind distribution of a typhoon around Taiwan and weakening wind speeds. The resulting waves decay because of the weakened winds. The interaction between the typhoon winds and the land is so complex that so far, it is difficult to accurately calculate the wind speeds inside the typhoon located around the land from the existing parametric wind models. Thus, the corresponding waves become functionally unpredicted. As ocean wave models are very sensitive to errors in the wind field, a new and extensive set of data, such as satellite measurements of wind and wave fields, provide model results with the best fit to the observations [13–15].

Artificial neural networks (ANN) should be regarded as a further extension of fitting to large observations as opposed to model-based attempts to estimate and predict wave behavior. However, an ANN does not provide insight into wave propagation processes that are provided by full-scale numerical models. The advantages of an ANN include computational efficiency and potentially greater predictive power, especially for non-linear problems, without the need for detailed geographic information. Thus, ANN has been used for numerous applications in different science and engineering fields.

Deo and Sridhar Naidu [16] used a neural network to make a real-time wave forecast based on leading observations of waves at a point. Deo et al. [17] proposed a feed-forward neural network to obtain wave heights and wave periods from the input of generated wind speeds. Deo and Jagdale [18] applied the neural network technique to accurately predict breaking height and water depth. Ziemianski [19] presented a hybrid method for wave propagation in which neural networks were applied to all nodes on the transmitting artificial boundary. Makarynskyy [20] presented two neural networks to improve short-term wave forecasts based on observations of wave heights and periods at two sites. Makarynskyy et al. [21] proposed two different neural networks to forecast wave heights and periods at Portugal. Chang and Chien [22] applied the multi-trend functions rather than the traditional transfer functions in neural networks used to fit the relationship between the inputs and the output and established an ANN wave model for typhoon waves. Chang and Chien [23] developed a neural-fuzzy model for simulating typhoon waves considering land effects. Kathrin et al. [24] applied a neural network associated with a cluster analysis to parameterize the exact non-linear interaction between source terms for wind wave spectra.

Chang and Chien [22,23] attempted to improve the accuracy of simulated typhoon waves by using neural network and neural-fuzzy network driven by the input of typhoon parameters such as central position, wind speed and moving velocity. However, one of predicted peaks of six typhoons in the verification for the neural-fuzzy network exceeded 1.4 m, while the difference from the observation and its corresponding relative error to the peak height was 0.35. This result indicates that the neural-fuzzy network from only inputs of typhoon parameters may provide divergent predictions for the peak typhoon waves when the typhoon goes along a path quite differently from those used in the training stage. Wave modelling provides an advantage from the results obtained by following the basic physical principle of wave propagation processes. An ANN directly relates the outputs to some resulting inputs by fast and efficient computation. Considering the advantages of both methods, the paper presents an ANN model for typhoon waves from several inputs, including relevant wind speeds and waves obtained by wave modelling. Section 2 briefly introduces the commonly used MIKE21_SW wave model. In Section 3, the input variables in the proposed ANN, including the model structure, are described. Data sources and model calibration and verification are demonstrated in Section 4. The conclusions are discussed in Section 5.

## 2. Wave models

The MIKE21_SW model [25], developed by DHI Water & Environment, is a type of WAN model that simulates the growth, decay and transformation of wind generated waves and swell in offshore and coastal areas. The fully spectral model governed by wave action equations was considered along with possible sources, such as wave dissipation due to white-capping; depth-induced wave breaking; bottom friction; wave growth by wind action; and energy transfer due to non-linear interactions between spectral components. These spectral components contribute to the modification of the spectrum during wind generation or the decay of wave motion. The MIKE21_SW model is widely used throughout the world for the assessment of wave climates in offshore and coastal areas in forecast and hindcast modes. Wind fields play a very dominant role in generating waves and thus it is important to get accurate estimates of this parameter. According to previous studies, the National Center for Environmental Prediction (NCEP) provides acceptable wind fields from successive reanalysis of global data assimilation and produces a database every 5 years or so that scientists can use to accurately calculate monsoon waves [26]. The resolution of NCEP is $1.875^\circ \times 1.875^\circ$, or approximately 200 km, which is too low to accurately simulate typhoon waves in a typhoon which likely forms a circular or elliptic shape with a common radius of 200–500 km due to the fast variation of typhoon winds.

The MIKE21 model considers a wind field consisting of rotational and translational components. At a distance, $r$, from the center of a typhoon, the rotational wind speed, $V_r$, is given as

$$V_r = \begin{cases} V_{\max}(r/r_m)^7 \exp(7(1-r/r_m)) & \text{for } r < r_m \\ V_{\max} \exp((0.0025 r_m + 0.05)(1-r/r_m)) & \text{for } r \geqslant r_m \end{cases} \quad (1)$$

where $r_m$ is the radius to the maximum winds, $V_{\max}$, in km, which are obtained from the website of the RSMC-Tokyo Center in Japan. Eq. (1) is similar to the Rankine vortex wind model (RVM) of Holland [27]. The value of $r_m$ can be estimated by Graham and Nunn [28]

$$r_m = 28.52 \tan h(0.0873(\phi - 28)) + 12.22/\exp(\Delta P/33.86) + 0.2 V_f + 37.22 \quad (2)$$

where $\phi$ is the latitude and $\Delta P$ is the atmospherical pressure depression between the ambient pressure, which can be assumed to be 1013.3 mb, at the periphery of the storm and the central pressure. The moving speed of a typhoon, $V_f$, leads to a translational component of the total wind speed, $V_t$, as in the equation

$$V_t = 0.5\ V_f \cos\varphi \quad (3)$$

where $\varphi$ is the angle between the radial arm and the line of maximum winds. The line of maximum winds occurs at an angle of 115° that is measured clockwise from a line extending from the center of the typhoon in the direction of the typhoon's movement, as shown in Fig. 1. The wind direction at a particular location is parallel to the tangent, except for a deflection angle turned in the direction of the wind towards the center of the typhoon. The deflection is caused by the friction between the water and air and is given as

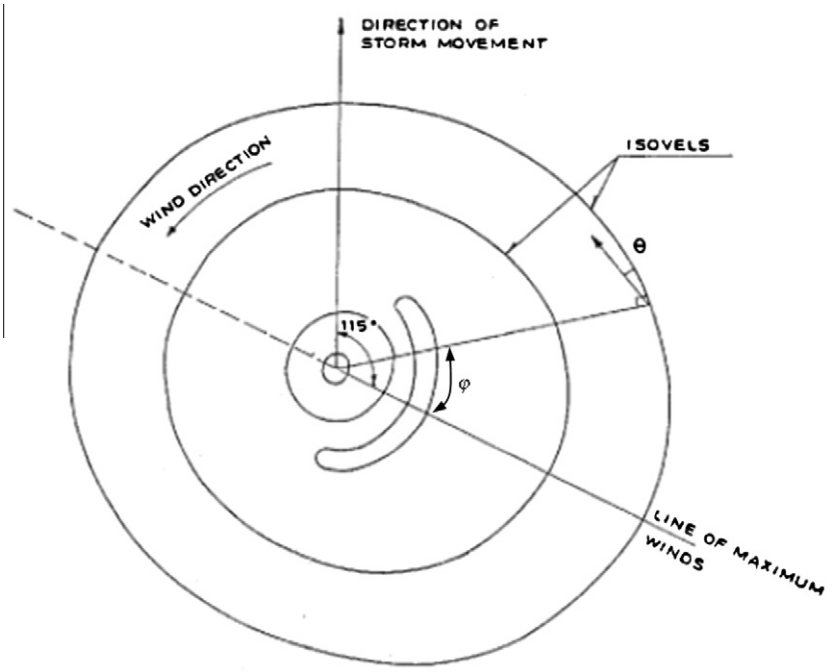


**Fig. 1.** The isotach pattern of a typhoon.

$$\theta = \begin{cases} 10^\circ & \text{for } 0 < r \leqslant r_m \\ 10^\circ + 15^\circ(r - r_m)/(0.2r_m) & \text{for } r_m < r \leqslant 1.2r_m \\ 25^\circ & \text{for } 1.2r_m < r \end{cases} \quad (4)$$

The resultant wind velocity inside the typhoon is $V_{RVM} = V_r + V_t$, using vector addition.

When the typhoon reaches Taiwan, the typhoon wind will become weak due to the land effect. So far, land effects on typhoon winds are still unpredictable so that no modification of Eq. (1) can be made when the typhoon is near Taiwan. The ANN model is chosen to remedy potential incorrect wave calculations owing to the land effect on the imperfect wind field. The proposed ANN model will be introduced in the next subsection.

Topographical information used in the MIKE21_SW model was derived from the ETOPO2v2 Global Gridded 2-min Database published by the National Geophysical Data Center (NGDC) [29]. ETOPO2v2 was created at NGDC from digital databases of seafloor and land elevations on a 2-min latitude/longitude grid. The computational domain, shown in Fig. 2, ranges from 111°E to 135°E and from 13°N to 31°N. Mainland china, Taiwan and parts of the Philippines are included in the computational domain. In addition, 2147 finite elements with 1173 nodes are gridded using the cell-centered finite volume method by automatically applying the optimal grid technique provided by the MIKE21_SW model. An unstructured mesh is used in the geographical domain (i.e., fine grid sizes are used around Taiwan and coarse grid sizes are used away from Taiwan). The time integration is performed using a fractional step approach where an explicit multi-sequence method is applied for the propagation of wave action.

A fully directional spectrum is used to compute wave–wave interactions and to represent the significant waves in the MIKE21_SW model for real irregular waves. The frequency domain of the wave spectrum was classified into 25 bands with a minimum frequency of 0.055 Hz and an increase rate of 1.1, indicating wave periods varying from 1.85 to 18.18 s. The computational time step is set by 15 min for the computational stability. All forcing sources except for tidal variation were considered in the MIKE21_SW model.

## 3. Backpropagation Neural Network

### 3.1. Model structure

A Backpropagation Neural Network (BPNN) was applied to modify the simulated waves from the MIKE21_SW model for fast and accurate calculations. A BPNN typically has three layers, namely an input layer, a hidden layer and an output layer. The number of input nodes is the same as the number of input parameters, and these input nodes receive data that are then passed onto the hidden layer nodes. These nodes individually sum up the received values after multiplying each input value by a weight. The nodes then attach a bias to this sum and pass on the result through a non-linear transfer function. The resulting transformed output from each output node forms the output vectors. The algorithm of a BPNN can be formulated by

$$\mathbf{O}_{N_O\times 1} = f(\mathbf{W}_{N_h\times N_i}\mathbf{I}_{N_i\times 1} + \mathbf{b}_{N_h\times 1}) \quad (5)$$

where $\mathbf{W}_{N_h\times N_i}$ and $\mathbf{b}_{N_h\times 1}$ are the matrices of the weights and of the biases between the input neurons, $\mathbf{I}_{N_i\times 1}$, and the hidden layer neurons, respectively, $f()$ is the transfer function, connecting the hidden layer neurons to output neurons, $\mathbf{O}_{N_O\times 1}$, and the subscripts $N_i$, $N_h$, and $N_o$ are the number of neurons of the input, hidden and output layers, respectively. The hyperbolic tangent sigmoid transfer function, $f(x) = \tan h\,(x)$ is chosen as the transfer function. For sigmoid units, the output varies continuously but not linearly as the input changes. Thus, sigmoid units bear a greater resemblance to real neurons than do linear or threshold units.

For common engineering problems, the number of hidden layers is suggested to be one, which is not complicated and is highly non-linear [30–33]. Thus, one hidden layer is used in the proposed ANN model. The number of neurons in the hidden layer is recommended by Huang and Foo [34] as

$$N_h = 2N_i + 1 \quad (6)$$

The objective of a BPNN is to minimize the global error between the transformed output and the observed data so that the properly trained BPNN tends to generate reasonable outputs when inputs

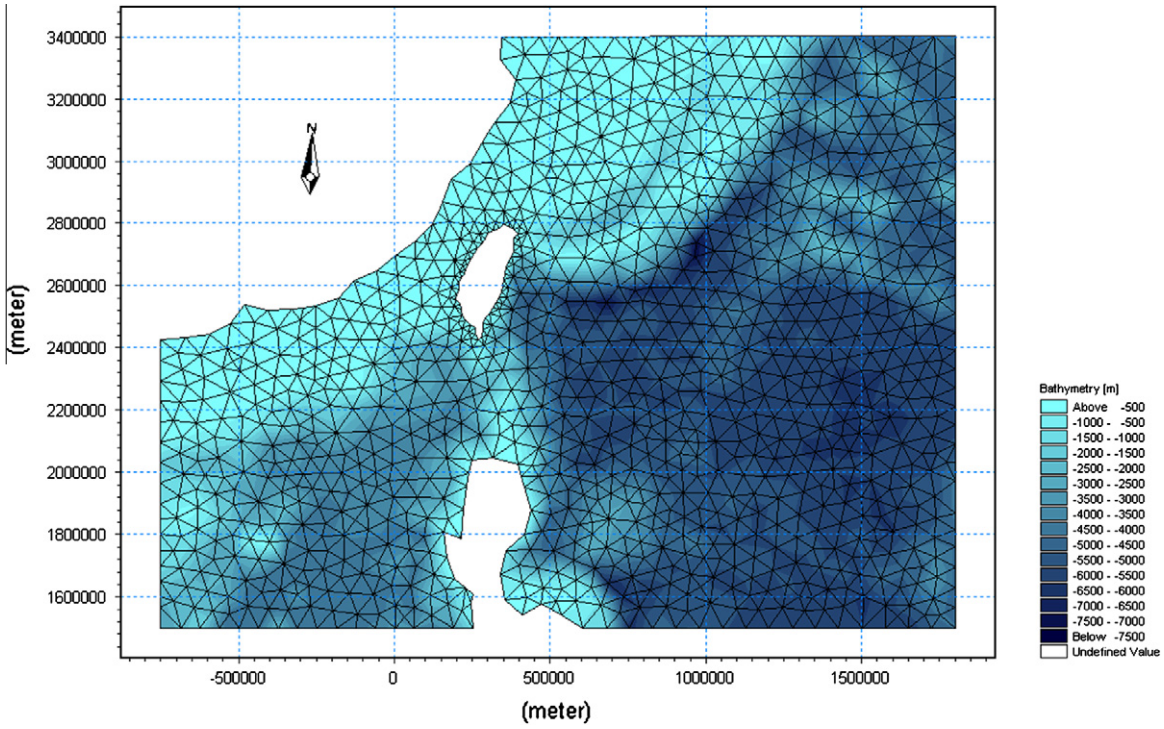


**Fig. 2.** Computational grids and topographical map.

are provided. The squared difference between the desired response, $H_m$, and the network response, $\mathbf{O}_{N_O\times 1}$, states that the training error, $E$, and can be written as

$$E = \frac{1}{N}\sum_{i=1}^{N}(\mathbf{O}_{P\times 1}(t_i) - H_m(t_i))^2 \tag{7}$$

When the errors of each iteration in both the learning stage and the verification stage decrease simultaneously, the model continues to learn. Conversely, whenever the error is magnified, the model stops learning. When the simulation error reaches the assigned minimum, the optimal weight and the bias matrices are set. Like the quasi-Newton methods, the Levenberg–Marquardt algorithm was designed to approach a second-order training speed without having to compute the Hessian matrix. This algorithm appears to be the fastest method for training moderate-sized feed-forward neural networks (up to several hundred weights [35]). Thus the 'trainbr' network training function in the Matlab software that updates the weight and bias values according to a Levenberg–Marquardt optimization is used in the present model. This function minimizes a combination of squared errors and weights, and then determines the correct combination so as to produce a network that generalizes well. The process is called Bayesian regularization and modifies the linear combination so that at the end of training, the resulting network has good generalization qualities. Training stops when one of the conditions, default values of training parameters in the Matlab software, is observed.

Whether the energy of wind waves rises or decreases depends largely on the energy input from the winds. Thus, the key to calculating the typhoon waves is to accurately evaluate the local wind speeds in a typhoon. The local wind speed can be measured at an observation station. Therefore, local wind speeds during the time period of a typhoon from the start to the disappearance of the typhoon as determined by NCEP and RVM, respectively, were chosen as input parameters, denoted by $V_{NCEP}$ and $V_{RVM}$, respectively. The performance of the MIKE21_SW model driven by the NCEP wind field was developed for a typhoon far from the point of interest and was driven by RVM for a typhoon near that location. Computed wind waves at the point of interest indicated the integrated performance of wave propagation and transformation based on physical processes. Thus, the significant waves calculated by the MIKE21_SW model, denoted by $H_{NCEP}$ and $H_{RVM}$, respectively, with energy source input by NCEP and RVM wind fields, respectively, were also chosen as input parameters. Four input parameters were used in the input layer. Following Eq. (6), nine neurons in the hidden layer were examined and found to be valid during the model calibration and verification. Wave height was one of the output neurons. The whole neural network structure of the present study is shown in Fig. 3.

### 3.2. Wave data

The wave data were collected by the Harbor and Marine Technology Center (HMTC), Ministry of Transportation and Communications, Taiwan, at 23°58′00″N, 121°37′30″E located at a distance of 380 m from the end of the eastern breakwater of Hualien harbor. The instrument used to measure waves was the Acoustic Wave and Current Profiler (AWCP) developed by the NORTEK instrumentation company in Norway. The mean water depth at this location is approximately −34 m. The location of wave measurement at Hualien harbor by HMTC is shown in Fig. 4. The typhoon data were collected from the RSMC-Tokyo Center in Japan. There were 51 typhoons between 2000 and 2006 that occurred in the western Pacific Ocean and passed through or by Taiwan according to reports from the Central Weather Bureau (CWB) of Taiwan. Among these, wave data were collected during only 33 of the typhoons due to missing data for some of typhoons during the observation period. Thus, 33 sets of simultaneously available wind and wave data were used as input data for the present ANN model.

The data on the typhoon's position and scale were obtained from RSMC-Tokyo Center and Coordinated Universal Time (UTC +8 for Taiwan) was used. The typhoon data were sampled every 6 h. A cubic spline interpolation was used to transform 6 h of

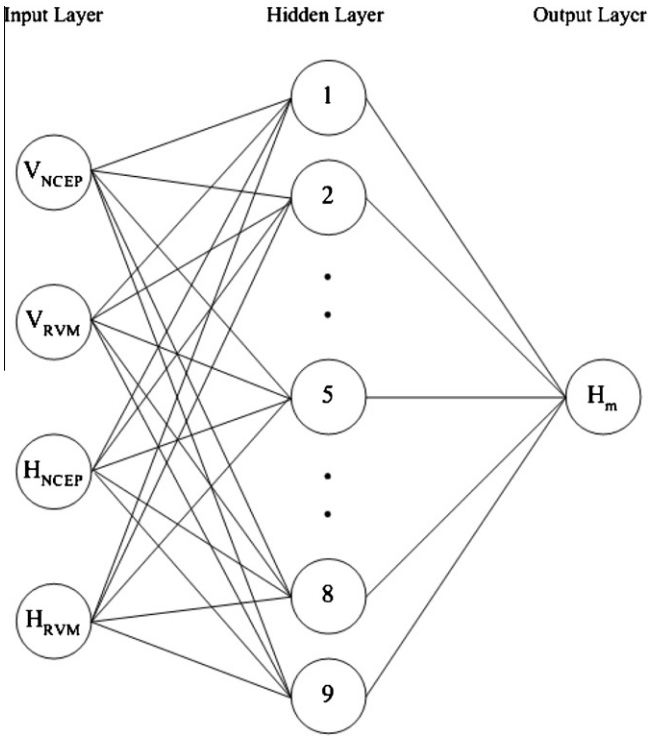


**Fig. 3.** Sketch of the construction of the proposed neural network.

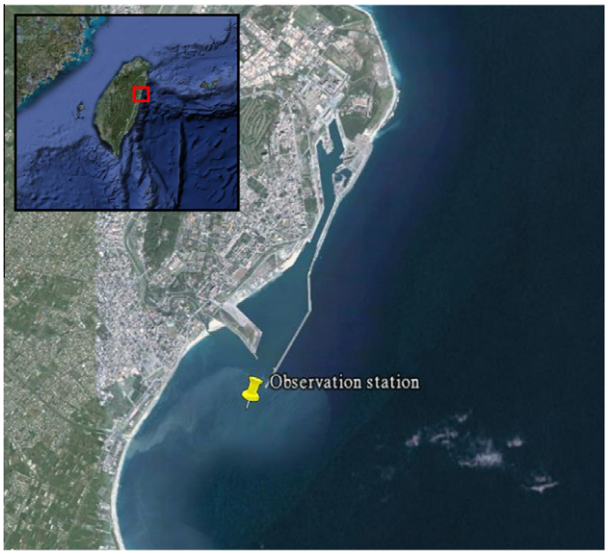


**Fig. 4.** The location of wave measurements taken at Hualien harbor by HMTC.

typhoon data into 1 h of data in order to make the data comparable to the 1-h wave data.

### 3.3. Indices of simulation performance

Typically, an applicable BPNN model should be validated in both the training stage and the verification stage. Commonly, the simulation performance of a model is evaluated by the root mean squared error (*RMSE*) and through the use of the correlation coefficients (*R*). The root mean squared error is defined as

$$RMSE = \sqrt{\frac{1}{n}\sum_{n}((H_{s,obs})_n - (H_{s,num})_n)^2} \quad (8)$$

where $H_{s,obs}$ and $H_{s,num}$ represent the observed and calculated wave heights, respectively, and $n$ is the total number of data measurements. The correlation coefficient of each typhoon signifies the degree of correlation between $H_{s,obs}$ and $H_{s,num}$. The maximum wave height and its occurrence time are very important in practical engineering. Two alternative indices of simulation performance are given by the difference between the peak observed wave height and the corresponding calculated value, $\Delta H_{s,p}$, and by the time lag between the corresponding times, $\Delta t_p$, as follows:

$$\Delta H_{s,p} = MAX(H_{s,num}) - MAX(H_{s,obs}) \quad (9)$$

$$\Delta t_p = t_{p,num} - t_{p,obs} \quad (10)$$

In this equation, $t_{p,obs}$ and $t_{p,num}$ are the times of the observed and calculated peak wave heights, respectively, and $\Delta t_p$ is the time difference.

## 4. Model validity

### 4.1. Model calibration

According to the scales and paths of the typhoons, 25 typhoons among 33 selected typhoons were depicted in Fig. 5 and were chosen for the training stage while the other eight typhoons, shown in Fig. 6, were used for model verification. All low atmospheric pressure and tropical cyclones were not considered so the proposed models cannot be used to model waves caused by monsoons. Figs. 5 and 6 indicate the paths of these typhoons that commonly start very far from Taiwan in the south-east and move towards the west or to north-west. The peak wave height of each typhoon used for the training model is shown in Fig. 7 and indicates that the largest wave was 10.85 m in height, and the smallest had a height of 1.61 m. The mean peak wave height was 4.30 m.

The total number of hourly wave data of 25 typhoons selected for the training stage is 5479. Four kinds of input data associated with output data of observed wave heights are used to obtain optimal weights and bias of the BANN model. The training process stops at the condition of maximum $\mu$ of Levenberg–Marquardt optimization occurring ahead other five conditions with their default values in the 'trainbr' neural network toolbox of the Matlab software.

The scatter plot of estimated and observed wave heights is shown in Fig. 8. The correlation coefficient and *RMSE* between estimated and observed wave heights is 0.898 and 0.419 m for whole

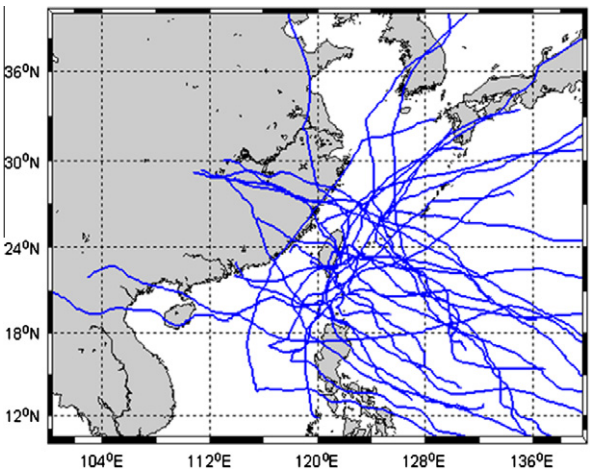


**Fig. 5.** The paths of 25 typhoons that passed through or by Taiwan during 2000–2006 and were used for model calibration.

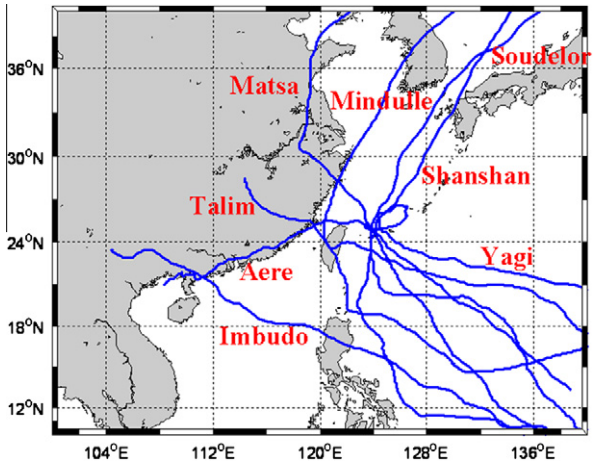


**Fig. 6.** The paths of eight typhoons used for model verification during 2000–2006.

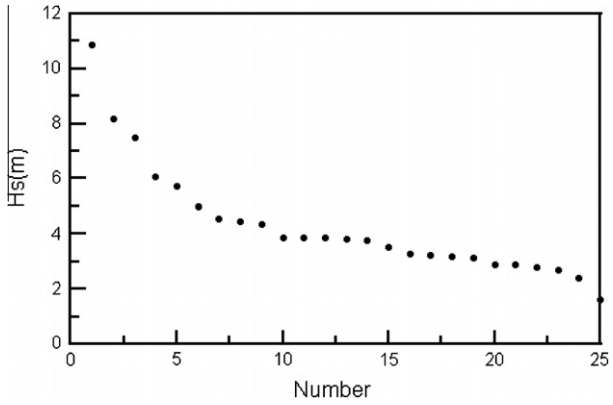


**Fig. 7.** The distribution of peak wave heights of data used for model training.

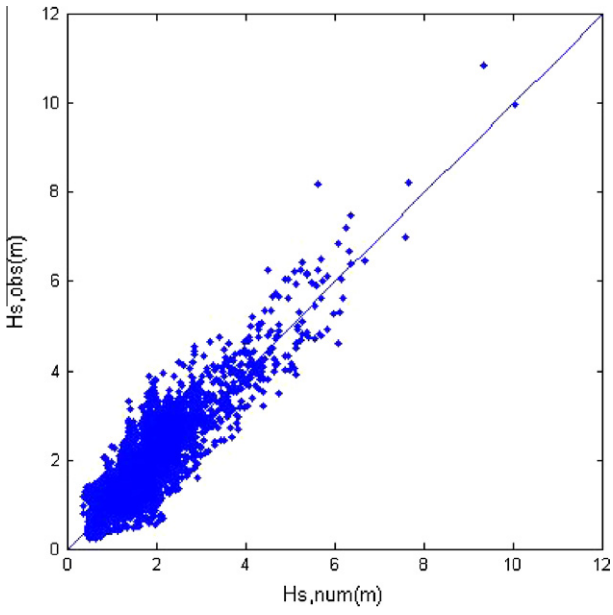


**Fig. 8.** Scatter plot of estimated and observed wave heights of 25 selected typhoons in model training.

data. High correlation coefficient and low *RMSE* shows excellent validity of model calibration.

### 4.2. Model verification

The four criteria were listed in Table 1 for eight cases of model verification. Here, four typhoons, Yagi (2000), Mindulle (2004), Matsa (2005), Shanshan (2006), were selected to indicate the performance of the time series of the calculated and observed wave heights shown in Figs. 9–12, respectively. In these figures, the solid lines denote the calculated wave heights simulated by the proposed ANN model and the dashed lines represent those by the MIKE21_SW model.

After Typhoon Yagi (2000) was formed on 21 October at a position of (145.9°E, 20.1°N), very far to the eastern of Taiwan, it moved to the west until it reached the northeastern waters of Taiwan at noon on 25 October. Throughout the duration of the typhoon, the maximum wind speed was 33 m/s. After 25 October, Typhoon Yagi weakened and made a U-turn to the north-east and moved slowly for 2 days. Typhoon Yagi dissipated after 27 October. The path of Typhoon Yagi is shown in Fig. 6. Fig. 9 plots the observed and computed heights of the waves. When Typhoon Yagi arrived in Taiwan, Hualien harbor was located under the left half of the typhoon. The wave heights computed by both models for the period in which wind waves grew exceeded the observed heights by approximately 0.5 m. However, when Typhoon Yagi approached Taiwan and moved slowly, the computed wave height by the MIKE21_SW model was higher than the observed height by 1.09 m due to the accumulated wind energy input. Both computed and observed heights showed the wave decay for the typhoon's departure. The simulated wave heights by the proposed ANN model were similar to the observed heights by *RMSE* = 0.38 m, or approximately half of that of the MIKE21_SW model. The proposed ANN model simulates a peak by a difference of 0.08 m with the actual peak observed at a 5 h delay.

Typhoon Mindulle (2004) was formed on 23 June south-east of Taiwan and moved to the west for 5 days. In 30 June, Typhoon Mindulle made a right-angled turn in the waters to the north of the Philippines, at approximately (122.0°E, 19.6°N), then passed over Taiwan and then proceeded northwards after 2 July. The maximum wind speed during Typhoon Mindulle reached 45 m/s. As Typhoon Mindulle approached Taiwan, the Hualien harbor was in the right side of the storm. Fig. 10 shows the observed and computed wave heights. The MIKE21_SW model accurately simulated the rapid increase in wave height until 29 June, and then produced a poor prediction between 30 June and 2 July. The large difference of 3.5 m results from the invalid wind field without considering the land effect. The wind speed was actually very much reduced very much over the high mountains along central Taiwan. When Typhoon Mindulle left Taiwan, the computed decaying wave heights agreed fairly well with the observed wave heights. Thus, the computed peak height agreed well with the observed peak wave height, which had a value of 5.50 m and differed by only 0.23 m from the computed peak. However, the time of computed peak occurred 36 h before the observed peak. The present ANN model provides a reliable measurement of the peak height, with an error of 0.39 m and shows no delay in the occurrence time of the data. The *RMSE* value of 0.62 m between the heights computed by the proposed ANN model and the observed heights for the whole period were less than *RMSE* = 0.96 m of the MIKE21_SW model.

According to Fig. 6, Typhoon Matsa (2005) moved to Taiwan from the south-east and then moved towards China. The path of Typhoon Matsa appeared to be a straight line. Typhoon Matsa traveled from 31 July to 9 August. Typhoon Matsa strengthened during the period from 3 August to 5 August and had a maximum wind speed of 40 m/s. Hualien harbor was located on the left side of Typhoon Matsa throughout the duration of this storm. Fig. 11 shows the computed and observed wave heights for Typhoon Matsa. As the waves grow, the wave heights computed by the

**Table 1**
Four performance indices of the results computed for eight typhoons in the verification stage.

| Year | | 2006 | 2005 | | 2004 | | 2003 | | 2000 |
|---|---|---|---|---|---|---|---|---|---|
| Name of typhoon | | Shanshan | Talim | Matsa | Aere | Mindulle | Imbudo | Soudelor | Yagi |
| $H_{s,p}$ (m) | | 4.24 | 7.53 | 3.18 | 3.68 | 5.50 | 3.71 | 3.71 | 2.55 |
| R | SW | 0.31 | 0.91 | 0.92 | 0.78 | 0.74 | 0.90 | 0.86 | 0.83 |
| | ANN | 0.72 | 0.94 | 0.91 | 0.74 | 0.85 | 0.91 | 0.91 | 0.81 |
| *RMSE* (m) | SW | 0.83 | 0.68 | 0.45 | 0.58 | 0.96 | 0.80 | 0.40 | 0.73 |
| | ANN | 0.56 | 0.56 | 0.30 | 0.53 | 0.62 | 0.51 | 0.41 | 0.38 |
| $\Delta H_{s,p}$ (m) | SW | −1.28 | −2.09 | 0.59 | 0.15 | −0.23 | 2.09 | −0.80 | 1.09 |
| | ANN | −0.33 | −0.76 | −0.16 | −0.11 | −0.39 | 0.73 | −0.82 | −0.08 |
| $\Delta t_p$ (hr) | SW | −143 | 10 | −13 | 3 | −36 | 0 | −9 | 10 |
| | ANN | 0 | −3 | 6 | 7 | 0 | 0 | −3 | 5 |

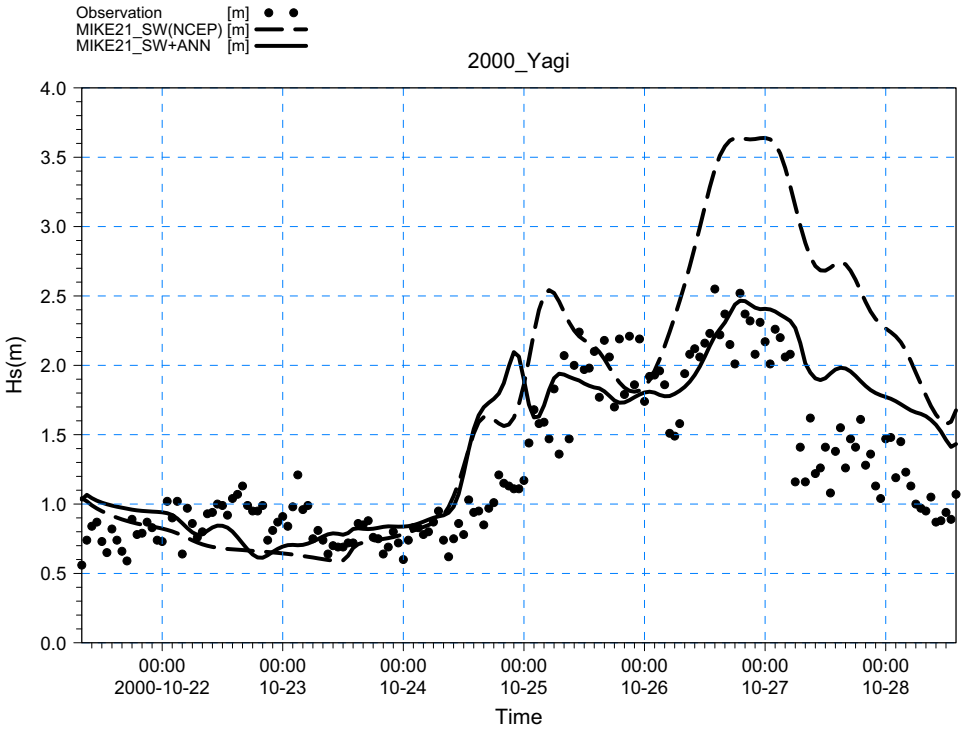


**Fig. 9.** The measured and simulated wave heights for Typhoon Yagi (2000).

MIKE21_SW model agree fairly well with the observed heights ahead the peak. The peaks simulated by the MIKE21_SW model were ahead by 13 h and showed a deviation from the observed peak of approximately 0.59 m. When Typhoon Matsa passed by Taiwan after 4 August, a decline in the waves was observed and the heights were approximately 1 m smaller than those computed by the MIKE21_SW model. During this period, wind speeds obtained by the RVM model exceeded the actual wind speeds that were weakened by the shelter of the islands. Although the proposed ANN model poorly simulated the occurrence time of the peak due to a 6 h delay, the calculated peak was close to the observed peak.

Fig. 6 indicates that Typhoon Shanshan (2006) traveled in a noticeably different path for 11 days. Typhoon Shanshan started on 9 September at a position (138.7°E, 13.3°N) far to the southeast of Taiwan and moved towards the northwest with gradual increase in wind speed until 12 September. After this time, Typhoon Shanshan moved west for 2 days and made a right-angle turn to move along the eastern waters of Taiwan. On 16 September, Typhoon Shanshan stayed in offshore waters northeast of Taiwan for a while, became weak and moved to Japan. Typhoon Shanshan had a maximum wind speed of 43 m/s on 15 September. Hualien harbor was located in the left half of Typhoon Shanshan throughout the duration of the storm. Fig. 12 shows the computed and observed wave heights for Typhoon Shanshan. Before 15 September, the wave heights located within Typhoon Shanshan varied significantly and moved with a different wind speed and a large change in direction. The MIKE21_SW model had a small peak on 10 September which exceeded the observed peak by 1 m. The observed peak was 4.24 m and occurred at 8 pm on 15 September. The MIKE21_SW model did not produce simulations during the peak so the difference between the computed and observed heights at that time was 2.1 m. When Typhoon Shanshan began moving towards Japan, the waves decayed sharply for 13 h and deviated from the observed peak by approximately 0.59 m. The low correlation coefficient ($R = 0.31$) and the large *RMSE* of 0.83 m illustrates that the MIKE21_SW model produced poor calculations for all of the wave heights, including the physical quantity and performance trends. The proposed ANN model modifies the poor simulation of the MIKE21_SW model to reduce the

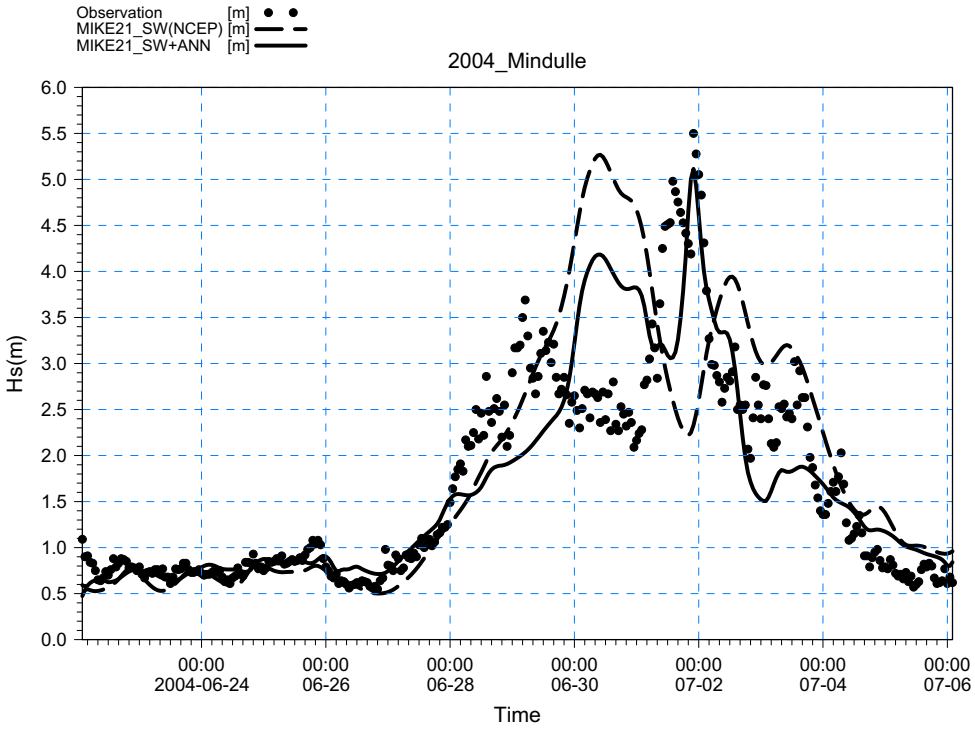


**Fig. 10.** The measured and simulated wave heights for Typhoon Mindulle (2004).

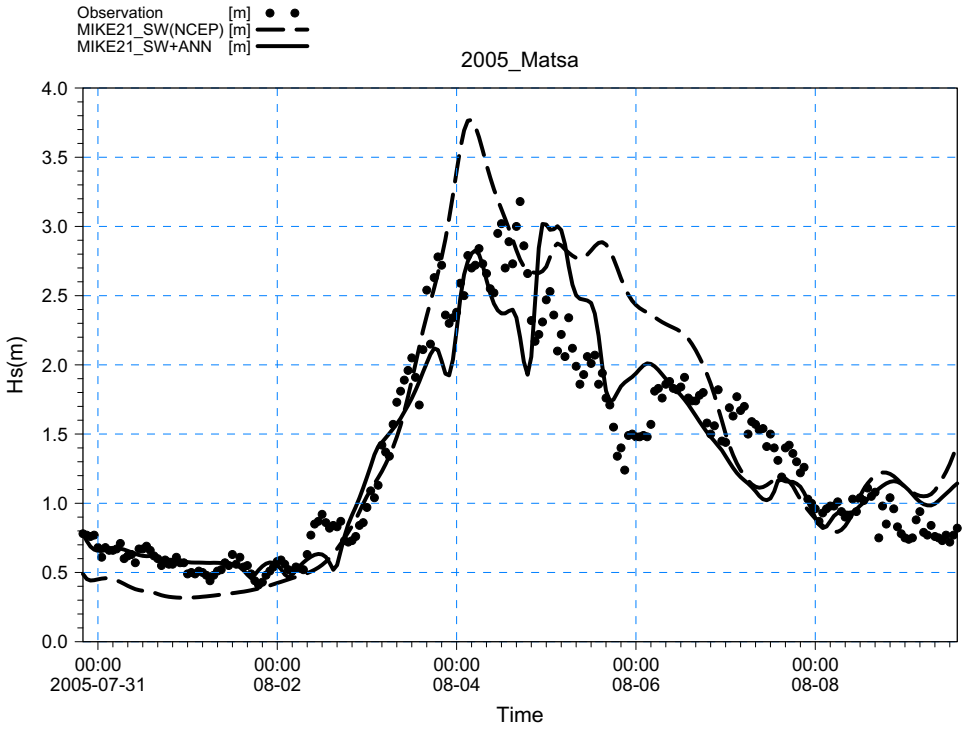


**Fig. 11.** The measured and simulated wave heights for Typhoon Matsa (2005).

number of incorrect peaks modeled and to enlarge the simulation at the true peak. Thus, the occurrence time of the calculated peak by the proposed ANN model coincides with that of the observed peak.

Van Vledder and Holthuisen [36] demonstrated that the WAM model still cannot accurately simulate waves in rapidly turning winds. Typhoons Yagi (2000), Mindulle (2004) and Shanshan (2006) made a U-turn or a right-angled turn during whole movement so that the MIKE21_SW model cannot give good predictions for these cases. However, the proposed ANN model properly improves the worse wave simulation by the MIKE21_SW model for these typhoons.

In all cases, when the typhoon is far from Taiwan, it has little effect on the waves at Hualien. The wave heights, such as the

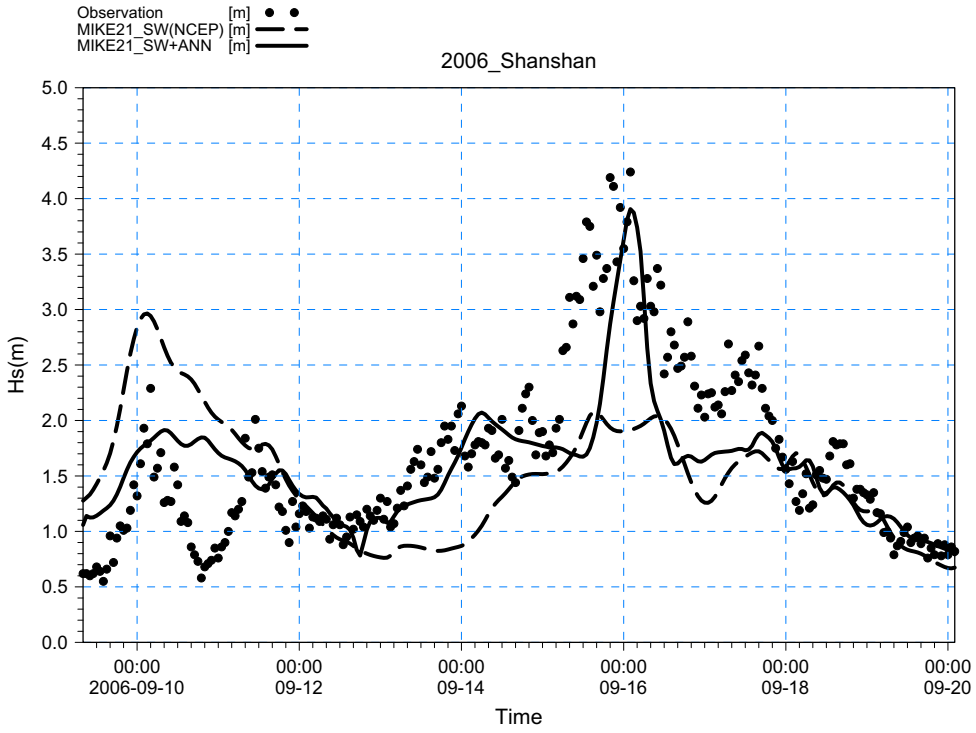


**Fig. 12.** The measured and simulated wave heights for Typhoon Shanshan (2006).

monsoon waves simulated by the MIKE21_SW model driven by the NCEP wind field, were close to the measured data so that the proposed ANN model had a slight promotion on such monsoon waves. The correlation coefficient exceeded 0.7 for both methods, indicating a good agreement with the measured data for the entire time series. The *RMSE* between estimated wave heights of each typhoon by the proposed ANN model and measured ones was ranged from 0.30 to 0.62 m, with a mean of 0.41 m that was smaller than that by the MIKE21_SW model, which had a mean of 0.68 m.

For the eight peak waves, Table 1 shows that the $\Delta H_{s,p}$ from the proposed ANN model ranged from −0.82 to 0.73 m, and that the absolute values had a mean of 0.38 m. The other $\Delta H_{s,p}$, produced from the MIKE21_SW model, ranged from −2.09 to 2.09 m. Those absolute values had a mean of 1.04 m. The former mean $\Delta H_{s,p}$ is smaller than the latter value, which demonstrates that the peak wave heights simulated from the proposed ANN model were superior to those produced by the MIKE21_SW model.

For the corresponding occurrence time of peak waves, $\Delta t_p$ produced from the proposed ANN model were within −3–7 h to the actual peak waves. The mean of the absolute values of $\Delta t_p$ was 3 h. The other $\Delta t_p$ produced by the MIKE21_SW model was within −143–10 h to the actual peak waves. Neglecting the largest time difference, the mean of the absolute values of the seven $\Delta t_p$ was 11.7 h. The former mean $\Delta t_p$ was also less than the latter value, indicating that the occurrence times of peak waves by the proposed ANN model was much more accurate than those produced by the MIKE21_SW model.

## 5. Conclusions

An average of three or four typhoons in 1 year pass through or by Taiwan according to data statistics on the paths of typhoons from 1897 to 2009 produced by the Central Weather Bureau (CWB) in Taiwan. Thus, information on swell and wind waves resulting from strong typhoons is very important for the safety of the people and marine structures, such as fishery and seawalls, in marine areas. Following the physical processes of wind waves from different energy sources, numerical models have been developed to accurately calculate water waves in the sea. The applicable Mike21_SW model was chosen to simulate typhoon waves in the open sea in order to produce accurate calculations. Due to land effects on typhoon waves around Taiwan, the ANN model provides a means of the calculations of typhoon waves currently produced when a typhoon is near Taiwan. The proposed ANN model is driven by local winds and waves simulated by the Mike21_SW model that considers the mechanism of wind waves and the physical process of wave propagation. Following the physical processes and key factors of wind waves, the proposed ANN model was found to provide good simulations of typhoon waves and modifications on some of the poor calculations produced by the Mike21_SW model. From the model verification, the proposed ANN model was found to produce accurate calculations of the peak of each typhoon with an average error of 0.38 m, while the occurrence time was delayed by an average of 3 h. The proposed ANN model has a higher correlation coefficient and a smaller *RMSE* than the Mike21_SW model and shows the whole computed waves of each typhoon are well consistent with observed waves.

## Acknowledgement

The authors would like to express their sincere acknowledgement to CECI engineering consultants Inc., Taiwan, under Grant No. 98932, for financial support.

## References

[1] Shore protection manual (SPM). US Army Coastal Engineering Research Center, Ford Beloir, vols. I–III; 1984.
[2] Hurdle DP, Stive MJF. Revision of SPM 1984 wave hindcast model to avoid inconsistencies in engineering applications. Coastal Eng 1989;12:339–57.
[3] Cardone VJ. On the structure of the marine surface wind field. 3rd International workshop of wave Hindcasting and Foracsting, Montreal, Quebec; 1992. p. 54–66.

[4] Resio DT. The estimation of a wind wave spectrum in a discrete spectral model. J Phys Oceanogr 1981;11:510–25.
[5] The WAMDI. Group the WAM model – a third generation ocean wave prediction model. J Phys Oceanogr 1988;18:1775–810.
[6] Hasselmann K, Barnett TP, Bouws E, Carlson H, Cartwright DE, Enke K, et al. Measurements of wind-wave growth and swell decay during the joint north sea wave project (JONSWAP), Dtsch Hydrogr Z 1973;12:A8.
[7] Booij N, Ris RC, Holthuijsen LH. A third generation wave model for coastal regions: part I. Model description and validation. J Geophys Res 1999;104:7649–66.
[8] Ris RC, Holthuijsen LH, Booij N. A third generation wave model for coastal regions: part II. Verification. J Geophys Res 1999;104:7667–81.
[9] Komen GJ, Cavaleri L, Donelan M, Hesselmann K, Hasselmann S, Janssen PAEM. Dynamics and modeling of ocean waves. Cambridge: Cambridge University Press; 1994. p. 532.
[10] Hsu TW, Ou SH, Liau JM. Hindcasting nearshore wind waves using a FEM code for SWAN. Coastal Eng 2005;52:177–95.
[11] Romeiser R. Global validity of the wave model WAM over a one-year period using Geosat wave height data. J Geophys Res 1993;98:4713–26.
[12] Liu PC, Schwab DJ, Jesen RE. Has wind-wave modelling reached its limit? Ocean Eng 2002;29:81–98.
[13] Jassen PAEM, Lionello P, Reistad M, Hollingsworth A. Hindcast and data assimilation studies with the WAM model during the Seasat period. J Geophys Res 1989;94:973–93.
[14] Lionello P, Gunther H, Jassen PAEM. Assimilation of altimeter data in a global third-generation wave model. J Geophys Res 1992;97:14453–74.
[15] Bauer E, Hasselmann S, Hasselmann K. Validation and assimilation of Seasar altimater wave heights using the WAM wave model. J Geophys Res 1992;97:12671–82.
[16] Deo MC, Shidhar Naidu C. Real time wave forecasting using neural networks. Ocean Eng 1999;26:191–203.
[17] Deo MC, Jha A, Chaphekar AS, Ravikant K. Neural networks for wave forecasting. Ocean Eng 2001;28:889–98.
[18] Deo MC, Jagdale SS. Prediction of breaking waves with neural networks. Ocean Eng 2003;30:1163–78.
[19] Ziemiański L. Hybrid neural network/finite element modelling of wave propagation in infinite domains. Comput Struct 2003;81:1099–109.
[20] Makarynskyy O. Improving wave predictions with artificial neural networks. Ocean Eng 2004;31:709–24.
[21] Makarynskyy O, Pires-Silva AA, Makarynska D, Ventura-Soares C. Artificial neural networks in wave prediction at the west coast of Portugal. Comput Geosci 2005;31:415–25.
[22] Chang HK, Chien WA. Neural network with multi-trend simulating transfer function for forecasting typhoon wave. Adv Eng Softw 2006;37:184–94.
[23] Chang HK, Chien WA. A fuzzy-neural hybrid system of simulating typhoon waves. Coastal Eng 2006;53:737–48.
[24] Kathrin W, Gunther H, Schiller H. Neural network parameterization of the mapping of wave spectra onto nonlinear four-wave interactions. Ocean Modell 2009;30:48–55.
[25] DHI, User guide and reference manual of MIKE 21-coastal hydraulics and oceanography hydrodynamic model. Danish Hydraulic Institute; 2009.
[26] Kalnay E, Kanamitsu M, Kistler R, Collins W, Deaven D, Gandin L, et al. The NCEP/NCAR 40-year reanalysis project. Bull Am Meteorol Soc 1996;77:437–70.
[27] Holland GJ. An analytical model of the wind and pressure profiles in hurricanes. Mon Weather Rev 1980;108:1212–8.
[28] Graham HE, Nunn DE. Meteorological conditions pertinent to standard project hurricane, Atlantic and Gulf Coasts of United States, national hurricane research project, report no. 3, US; 1959.
[29] ETOPO2v2 global gridded 2-minute database, National Geophysical Data Center, National Oceanic and Atmospheric Administration, US Dept Commerce. <http://www.ngdc.noaa.gov/mgg/global/etopo2.html>.
[30] Chester D. Why two hidden layers are better than one. In: Proceeding IEEE international joint conference on neural networks, Washington, DC; 1990. p. 265–8.
[31] Hayashi Y, Sakata M, Gallant SI. Multi-layer versus single-layer neural networks and an application to reading hand-stamped characters. In: Proceeding of international conference on neural networks. Paris; 1990. p. 781–4.
[32] Kurkova V. Kolmogorov's theorem and multilayer neural networks. Neural Networks 1992;5:501–6.
[33] Hush DR, Horne BG. Progress in supervised neural network: what's new since lippmann. IEEE Signal Process Mag 1993;10:8–39.
[34] Huang W, Foo S. Neural network modelling of salinity variation in Apalachicola River. Water Res 2002;36:356–62.
[35] Chang HK, Lin LC. Multi-point tidal prediction using artificial neural network with tide generating forces. Coastal Eng 2006;53:857–64.
[36] Van Vledder GP, Holthuisen LH. The directional response of ocean waves of turning winds. J Phys Oceanogr 1993;23:177–92.